Geotechnical Insights via Electrical Resistivity Imaging of Fault Zones

M. Akbariforouz
CEE, The Hong Kong PolyU, Hong Kong; EIT, Ningbo
Q. Zhao
CEE, The Hong Kong PolyU, Hong Kong
C. Zheng
EIT, Ningbo; SUSTech, Shenzhen

doi: https://doi.org/10.21467/proceedings.7.7.6

ABSTRACT

Hong Kong's unique topography, dense population, and lithology necessitate constructing and stabilizing numerous large-scale geoengineering projects, such as tunnels or rock slopes. The rock mass deformation modulus is essential for evaluating the bearing capacity and deformations. Deformation moduli measured through laboratory experiments, empirical equations, or even in situ tests can not present a representative elementary volume (D_{REV}) due to limited test coverage and technical difficulties in harsh geological or topographic conditions, such as near faults. This study utilized electrical resistivity (*ER*) tomography and numerical back-analysis to investigate D_{REV} near faults; we also employed geoelectrical contrasts to detect proper locations for installing extensometers along excavated galleries of rock slopes. The deformations recorded by extensometers were used to back-calculate the D_{REV} values by finite difference numerical modeling. We established a correlation between *ER* and D_{REV}, which was 30 to 80% more accurate than those obtained through conventional approaches. Our methodology provides a systematic approach to assess faulted rock mass behavior for various geoengineering projects, which is also replicable for other geological formations with harsh geology or limited access without exposing an extreme financial burden, technical challenges, or environmental issues.

1 INTRODUCTION

The landscape, high-density population, and geological features of Hong Kong require geoengineering structures like tunnels and slopes. Rock mass behavior for such projects must be investigated at the representative element volume (REV) or the smallest volume representing the whole medium's properties (Hill, 1963).

The rock mass deformation modulus is a scale-dependent parameter controlling the mechanical characteristics; this parameter is different at REV (D_{REV}) from the values obtained by conventional methods, such as empirical equations or laboratory and in situ tests (Aladejare & Idris, 2020; Brady & Brown, 1993), considering the limited coverage and unrepresentative interpretations.

Designing and constructing tunnels or slopes using inaccurate D_{REV} values resulted in extreme financial burdens and devastating impacts on human lives (Peng & Zhang, 2012). D_{REV} controls the bearing capacity and deformations under loading/unloading. The lithological conditions, fracture characteristics, rock strength parameters, water saturation, and the tested volume (i.e., scale impacts) affect D_{REV} (Aksoy et al., 2012;

Proceedings DOI: 10.21467/proceedings.7.7; Series: AIJR Proceedings; ISSN: 2582-3922; ISBN: 978-81-989164-3-3

Barnard & Heymann, 2015; Fattahi et al., 2019). Moreover, the excavation or blasting alters D_{REV} (Palmström & Singh, 2001). Therefore, the effects of these parameters on D_{REV} are pivotal.

Numerical back-analysis of deformations recorded by extensometers inside galleries or tunnels is an indirect, promising technique to evaluate D_{REV} (Ghotbi Ravandi et al., 2017; Khodabakhshi & Mortazavi, 2018; Ren et al., 2021); however, performing such a back-analysis is challenging due to the limited in situ data associated with financial concerns or technical difficulties. Moreover, assessing the locations of extensometers is essential for complete coverage of all rock mass conditions. If we can establish a relationship between numerical back analysis and geophysical tomography, it can mitigate such challenges by applying them to other study sites.

Geoelectrical resistivity tomography (*ER*) can cover a representative rock mass (Archie, 1947) as a necessary part of geoengineering projects without exposing the extra financial burden of in situ deformation measurements. The induced electrical current (I) between electrodes (K and L in Figure **1a**) causes potential differences (ΔV between voltmeters M and N) for different rock types (Figure **1b-c**) (Telford et al., 1990).

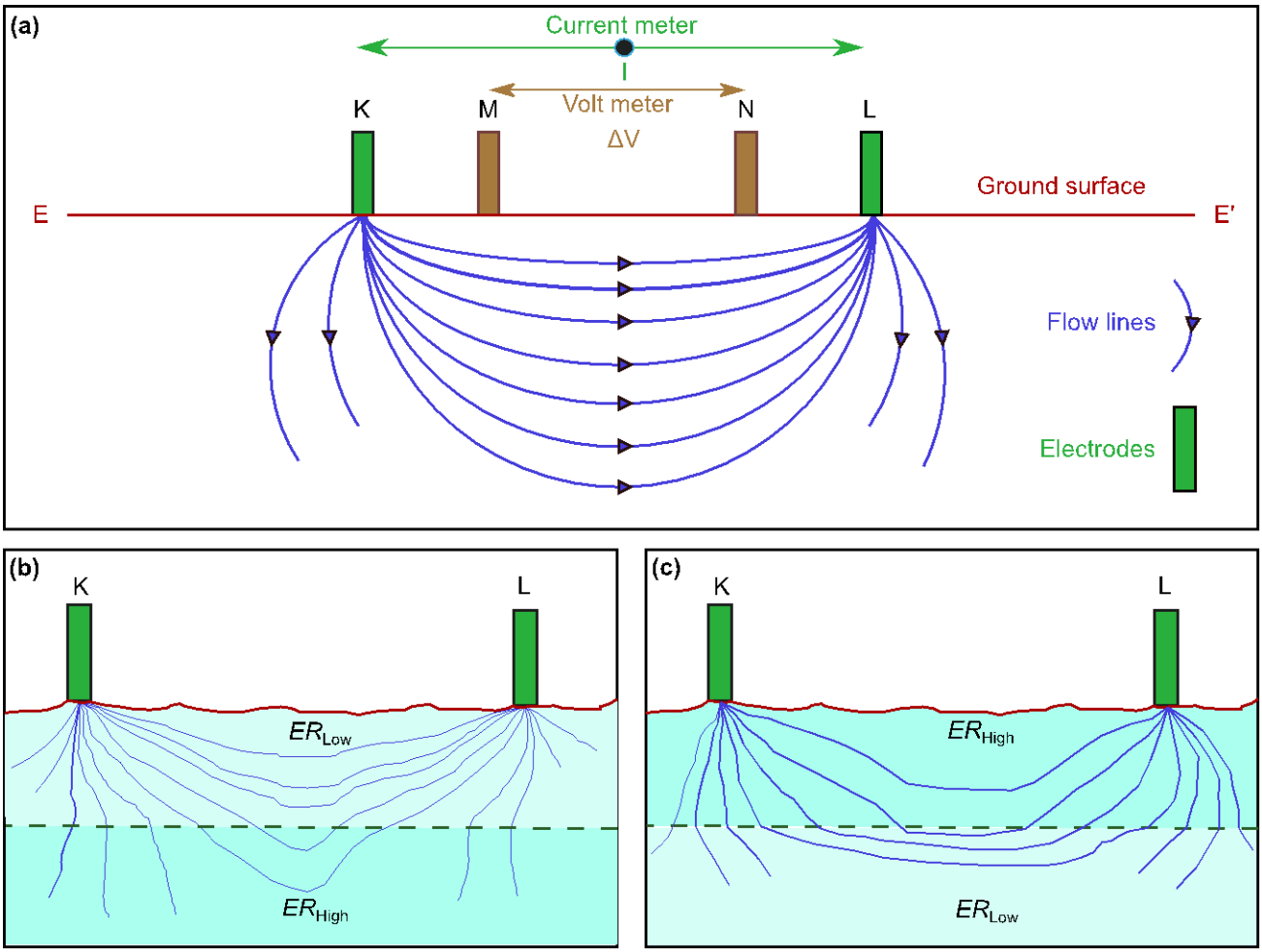

Figure 1: (a) Schematic view for electrical profiles (EE´) with voltmeters M & N and current electrodes K & L. The current is distorted for two rocks (ER_{Low} and ER_{High}) from a lower to higher *ER* (b) and a higher to lower *ER* (c) (modified from (Nia & Mahdavi, 2020)).

The effects of rock discontinuities (Akbariforouz et al., 2023; Carpenter et al., 2011; Li et al., 2015), lithology (Ammar & Kamal, 2018; Pazha et al., 2019), fluid saturation (Ammar & Kamal, 2018; Bhatt & Jain, 2014; Liu et al., 2023), stress regimes (Stavrakas et al., 2003; Triantis et al., 2006), and strength parameters on *ER* and rock mass deformations (Akbariforouz et al., 2022; Kahraman & Yeken, 2010; Ranjbar & Nasab, 2019) were consistent based on laboratory (Kahraman, 2022; Su & Momayez, 2017; Wang & Gelius, 2010) and field evaluations (Li et al., 2015; Pazha et al., 2019; Sandler et al., 2009). Therefore, *ER* variations can be used to assess the faulted rock mass deformations and D_{REV}.

The anomalies, such as cavities, conductive materials, or water-bearing areas, can result in misleading *ER* (Militzer et al., 1979; Rolia & Sutjiningsih, 2018); therefore, additional geophysical techniques must be applied to avoid such misinterpretations. We evaluated D_{REV} for a sedimentary formation by comparing numerical back-analysis of extensometers and *ER* tomography to develop an accurate, environmentally friendly, and financially affordable relationship for D_{REV}.

2 Methods

2.1 Studied Area and ER Tomography

The study site is a slope with 184 m height in the Asmari-Jahrum Formation (AJF) in the Central Plateau of Iran, consisting of thick-bedded carbonate rocks (Amirshahkarami et al., 2007). *ER* measurements were conducted by a Schlumberger array with a maximum length of 3 km and an electrode distance of 30-100. Around 100 electrodes were used along a 3000 m profile for 30 m distances. No igneous masses, conductive minerals, water-bearing structures, or cavities were detected in the study site based on the nuclear magnetic resonance and automated gravity meter up to 250 m depth (Howland-Rose, 1981).

2.2 In situ Tests

Plate-loading (1 m diameter with five extensometers at 0.095, 0.085, 1.79, 2.59, and 3.7 m depths) and dilatometer tests (3 up to 45 m depth and along boreholes with diameter = 10.1 cm) were performed at 2 m × 2 m galleries based on ISRM standards (ISRM, 1998; Ladanyi, 1987). The deformation modulus under loading (D_L) and unloading (D_U) was measured based on these tests. The loading cycles (minimum pressure from 0.5 to maximum 3 and 10 bar) were five for plate-loading and three for dilatometers.

2.3 Back-Analysis of Extensometers

Performing in situ tests at harsh topography or near faults, such as faults F1, F4, and F5 in the study site, is challenging. In galleries, anchor extensometers with an accuracy of $\pm$3μm were installed inside horizontal and vertical boreholes at 0.4-1 m distances from the gallery surface near faults and sharp *ER* variations.

For the numerical models (20 m × 20 m or ten times the gallery size), roller and XY-fixed (pins) boundaries were considered for sides and on the bottom (Figure **2**) with 100 meshes in each direction, ranging from coarse to fine meshes in the middle. Cohesion (C_{rm}) and friction angle (ϕ_{rm}) were assessed by the generalized Hoek-Brown failure criterion (Rocscience, 2007) using rock mass classification index (GIS), overburden (h), density (ρ), and rock index (m_i). The Poisson ratio of rock mass was considered 0.35 based on in situ tests and laboratory experiments.

Proceedings DOI: 10.21467/proceedings.7.7

Series: AIJR Proceedings
ISBN: 978-81-989164-3-3
ISSN: 2582-3922

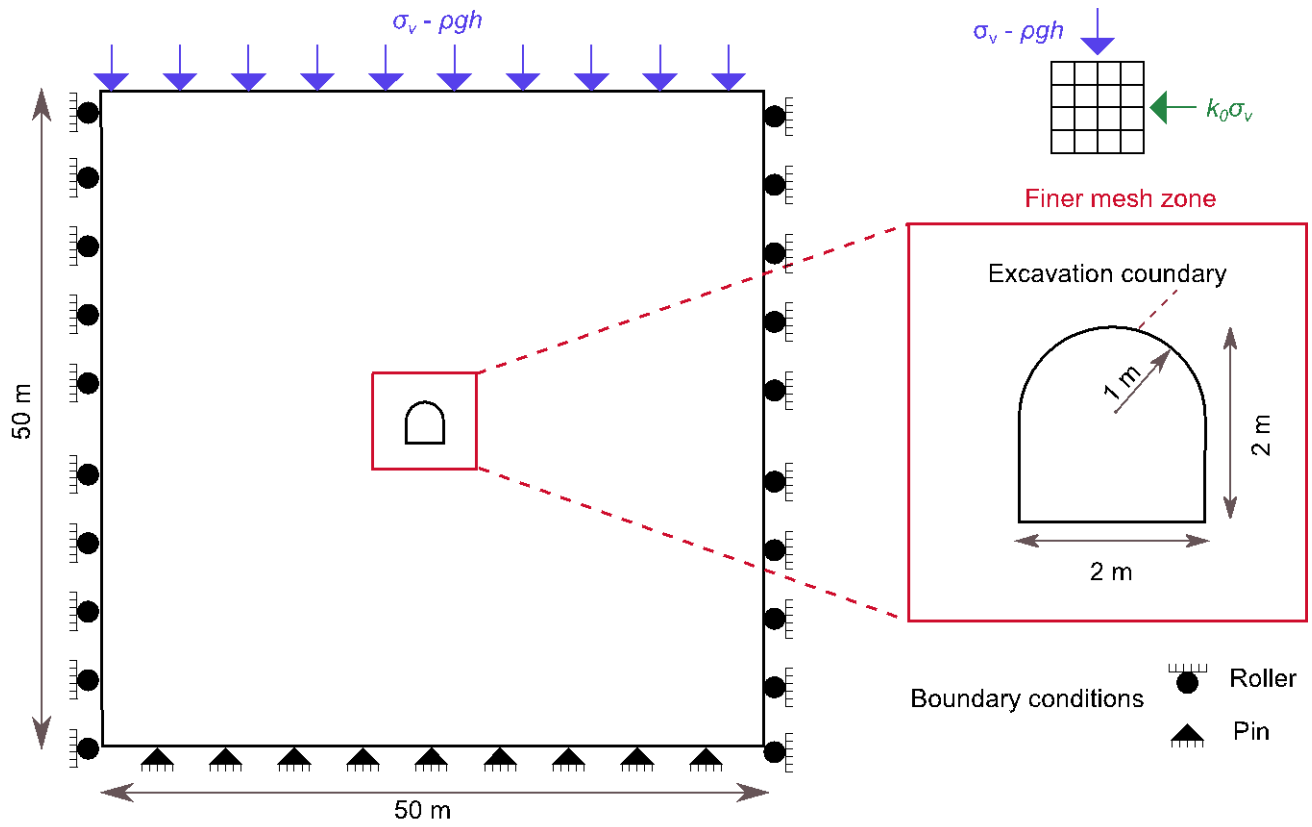

Figure 2. The boundaries, geometry, and parameters of numerical models, where σ_v and $k_0\sigma_v$ are the vertical and horizontal stress components, respectively. ρ, h, and g represent the density, overburden height, and gravity, respectively.

The deformation modulus under unloading at the REV ($D_{UREV} < D_U$ of in situ tests) was evaluated by a numerical back-analysis (FLAC^{2D}) (ITASCA, 2002), starting from D_U up to reaching a modulus that resulted in deformations recorded by the installed extensometer (Δ_{REV}). For D_{REV} under loading (D_{LREV}), the ratio of D_{UREV} by D_U (in situ tests) was used (i.e., $D_{LREV}=(D_{UREV}/D_U)\times D_L$), considering no alternative was available to evaluate D_{LREV}. The flowchart evaluating D_{REV} based on *ER* is shown in Figure **3**.

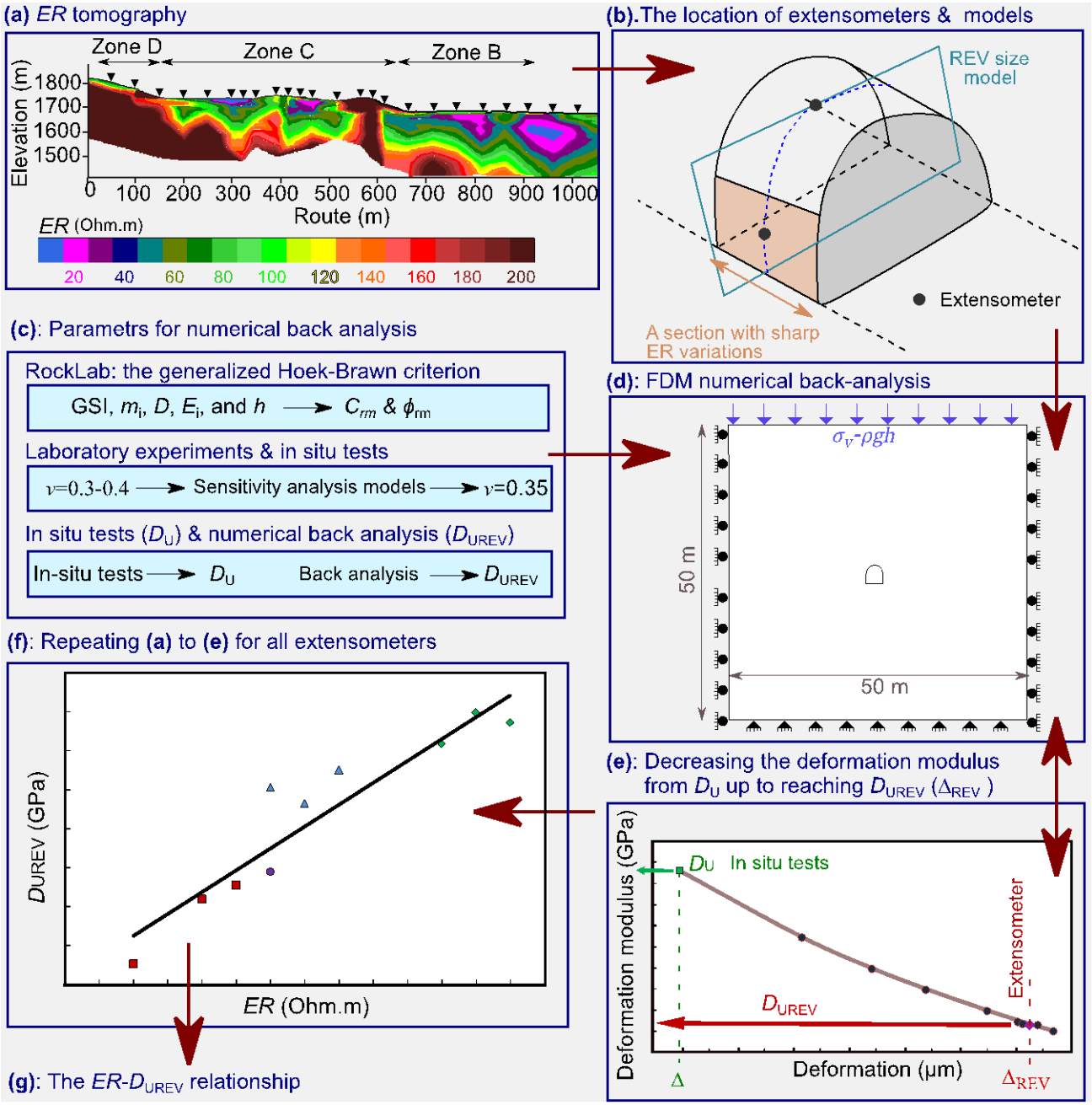

Figure 3. D_{REV} based on *ER*: (a) detecting extensometer locations extensometers based on sharp *ER* changes, (b) the deformations (Δ_{REV}) recorded along borehole extensometers, (c) rock mass parameters for the numerical models, (d) the FDM model, (e) back-analysis from D_L to D_{UREV} (reaching Δ_{REV}), (f) the back-analysis results for all extensometers, and (g) the *ER*-D_{UREV} criterion.

3 Results

The study site was divided into four lithological zones, and *ER* alterations were recorded for the whole study site. *ER* values in Zone A (dolomitic limestone) spanned from 100 to 160 Ω·m, except near F4 and F5 faults (60-100 Ω·m). We divided the excavated gallery (LG3) into five subsections with a 10-20 Ω·m variation and installed borehole extensometers for these subsections. At 15 and 40 distances, *ER* was 160-180 and 120-140 Ω·m, respectively. The *ER* range near Fault F4 (50 m from the gallery) was 100-120, while the range near the intersection of F4 and F5 faults (at 80 and 90 distances) was 80-100 and 60-80 Ω·m, respectively (Figure **4**). The *ER* range for Gallery LG1 was 20-100 for Zone B (marly limestone) and 100-200 Ω·m for Zone C (dolomitic limestone). The lowest *ER* values for Zone C were recorded near F1 at around 100 Ω·m. Two different layers with *ER* values of 20-60 and 60-100 Ω·m were detected within Zone B. *ER* varies between

Proceedings DOI: 10.21467/proceedings.7.7
ISBN: 978-81-989164-3-3

Series: AIJR Proceedings
ISSN: 2582-3922

120 and 200 Ω·m for Zone D (limestone).

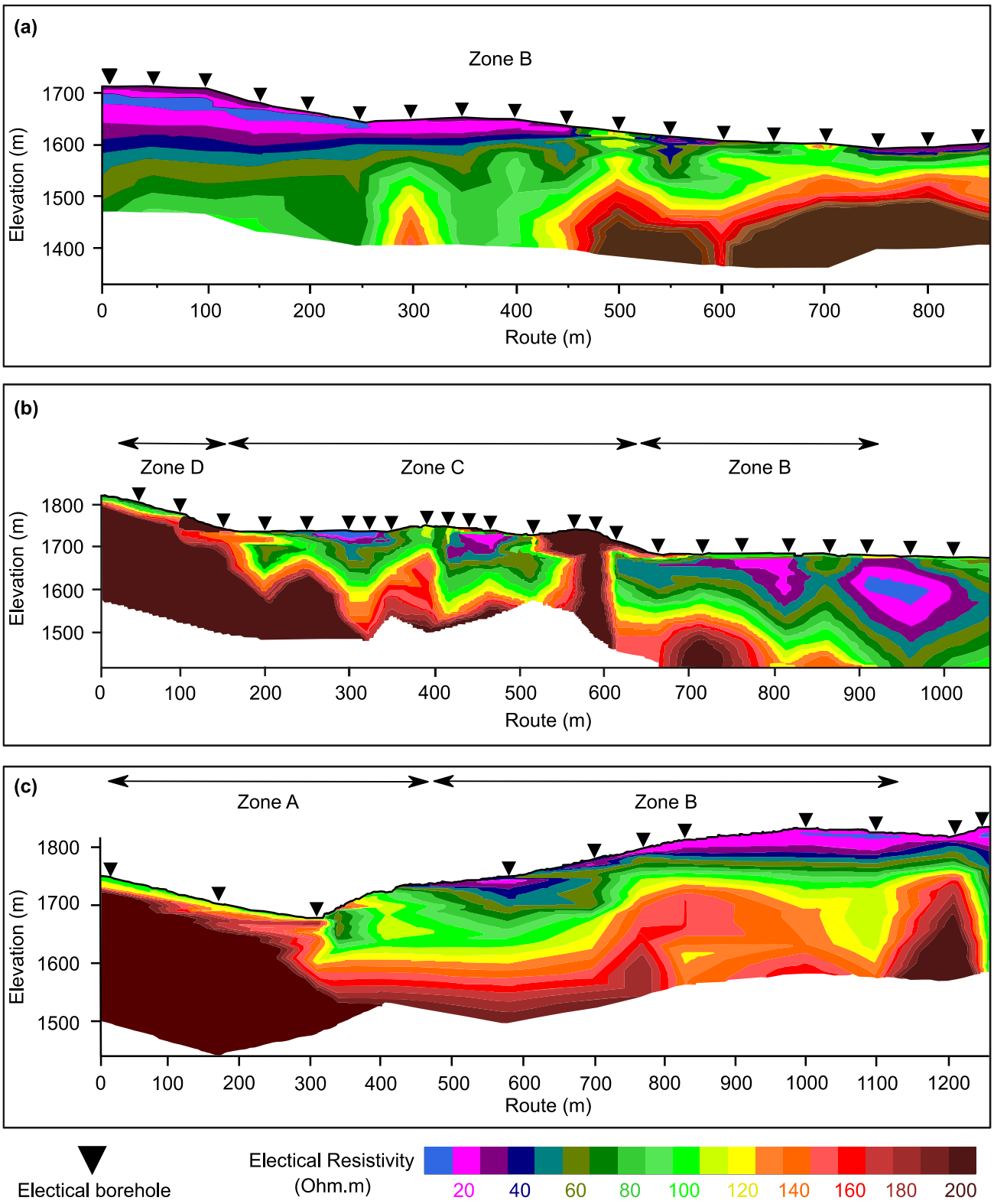

Figure 4. Electrical resistivity tomography for three profiles of the study site

A plastic area (0.25 to 0.5 m) was observed in the numerical models around the galleries for the extensometers; the extensometer deformations also displayed a higher difference between values recorded by equipment inside the plastic area (0.5 m). For example, Δ_{REV} for Zone A was 76 % (1354/1769μm) and 72 %

(859/1190μm) of Δ_{REV} outside this zone in horizontal and vertical boreholes, respectively. Therefore, extensometers outside the plastic area (60-100 cm from the gallery inlets) were utilized for measurements.

Figure **5** shows deformations for Extensometer 5 at LG1. First, the deformations based on the minimum D_U values of in situ tests (Δ) were calculated. For example, the minimum modulus was 4.73 GPa based on the plate-loading tests. Subsequently, deformations based on borehole extensometer (Δ_{REV}) were monitored for 120 days until reaching a variation below 10μm for extensometers at 60 cm to 100 cm (outside the plastic deformation zone) distances during the last month. D_{UREV} values were back-calculated based on the recorded Δ_{REV} by decreasing the deformation modulus (D_U) in numerical models until reaching deformations at a ±3μm span from Δ_{REV}.

We also assessed the sensitivity of deformations to Poison ratio (v); maximum deformations enhanced by 3.6 % (from 1989 to 2063μm) for a rise of v from 0.3 to 0.4 (33 %), while a relatively similar deformation modulus change (4.73 to 3.27 GPa) resulted in a deformation increase from 1397 to 2026 μm (31 %). Therefore, the influence of the deformation modulus on deformations was much higher than v, and a Poison ratio equal to 0.35 was employed for all models (same as in situ tests).

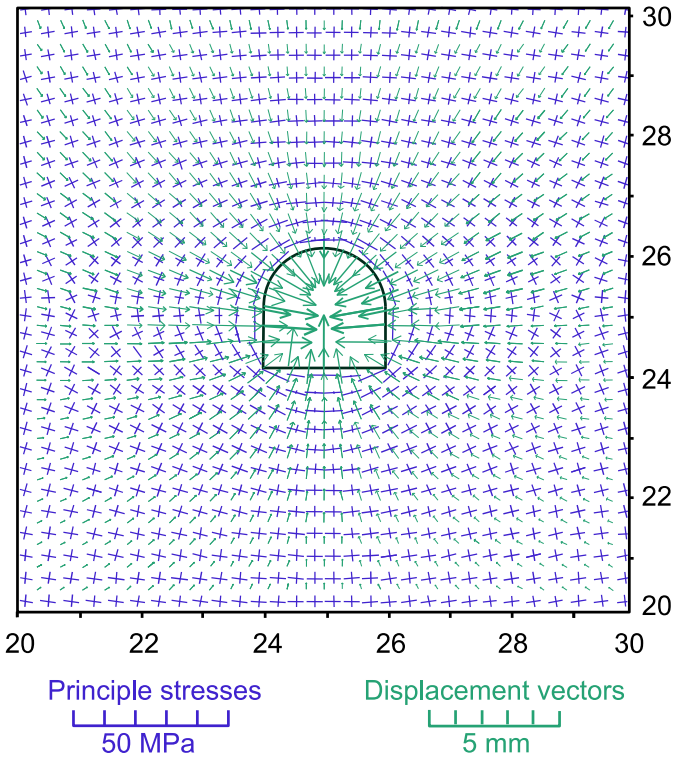

Figure 5. Numerical model (plot: 10 m × 10 m) with Δ_{REV} = 2026μm for the extensometer installed at 80 cm from the gallery span; D_{UREV} back-calculated as 3.27 GPa compared to the in situ tests (4.73 GPa).

We developed a relationship between ER and D_{UREV} based on all numerical models and back-calculated values with R^2 = 89.3 % (Equation (**1**)). We utilized this relationship to divide the rock masses at the dam axis into subsections based on sharp ER variations for Zones A to D, in addition to faulted rock masses (Figure **6**).

$$D_{UREV} = 0.028\ ER + 0.68 \qquad \textbf{(1)}$$

Proceedings DOI: 10.21467/proceedings.7.7

Series: AIJR Proceedings
ISBN: 978-81-989164-3-3
ISSN: 2582-3922

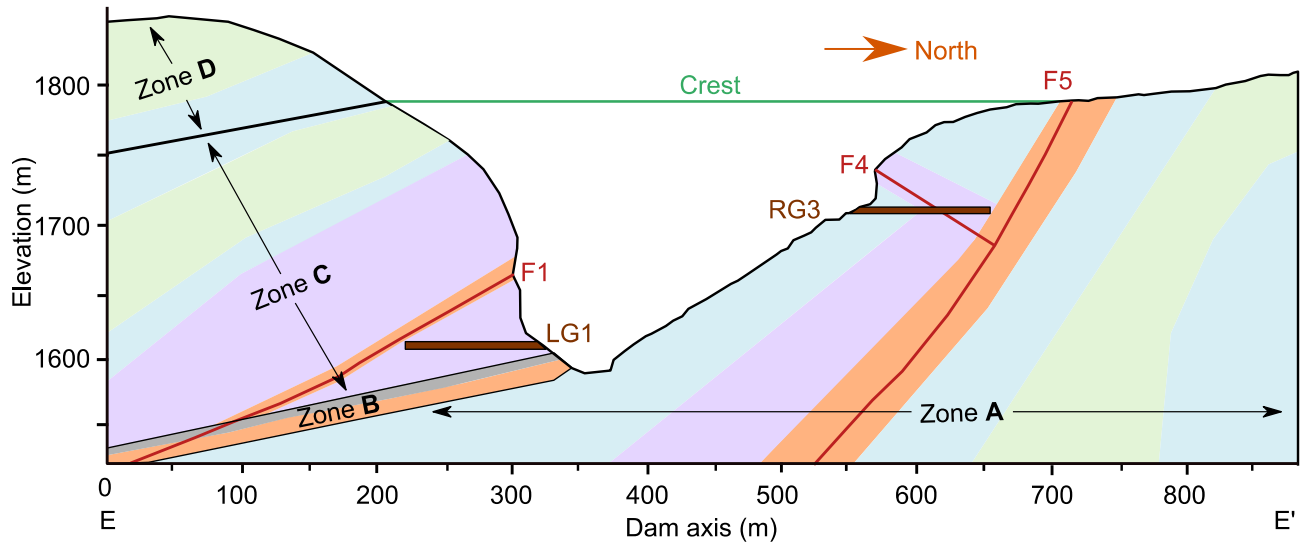

Symbol					
Subsection	I	II	III	IV	V
ER (Ohm.m)	160-200	120-160	100-120	60-100	20-60
D_{UREV} (GPa)	5.13-6.24	4.02-5.13	3.46-4.02	2.35-3.46	1.24-2.35

Figure 6. Ranges of *ER* and D_{UREV} values calculated using the methodology developed in this study for the whole dam axis: Zone A, C, and D are shown by the arrow. D_{UREV} variations within the slope and near faults are shown in the subsections.

4 Discussion

Our approach includes the influence of jointed area, faulted rocks, and weak bedding on the deformation modulus at REV, which is impossible for the in situ tests due to their limited coverage and technical challenges. The *ER*-D_{REV} correlation is proved based on previous laboratory and field-scale studies. Our results also confirm a direct relationship between *ER* and D_{REV}.

Moreover, geophysical prospecting is a common and affordable technique. Therefore, geoelectrical tomography can be a practical solution for evaluating characteristics of faulted rocks without adding extra financial burdens comparing numerous in situ tests. Geophysical methods are also fast, non-destructive, and environmentally friendly.

After elucidating the advantages of the developed technique in this study, explaining the limitations of this study is critical. We evaluate D_{REV} accurately and develop an *ER*-D_{REV} relationship using numerical back-analyses; nonetheless, extensometer data are often unavailable, particularly for small projects. However, Equation (**1**) can predict D_{REV} when no borehole extensometer data is available, particularly for similar sedimentary formations.

The *ER* range, lithology, and fault properties can affect the faulted rock mass conditions. The resolution of electrical data by a 30-50 m electrode distance is enough to detect the 20 m subsections with different D_{REV} values for a maximum depth of 250 m. Nonetheless, the provided *ER*-D_{REV} relationship cannot be used for igneous rocks or other sedimentary formations with *ER* higher than 200 Ω·m. However, this approach can be repeated for different projects by installing borehole extensometers based on *ER* contrasts.

Despite employing low electrode distance and complementary geophysical data, *ER* values can still suffer from variability. We consider a range of *ER* values (10 Ω·m) to control the model results, showing 5-25 % variability for different *ERs*; the effect of *ER* variability of 10 Ω·m is higher for lower *ER* ranges (10-30 Ω·m). A safety factor (e.g., 1.25) or a range of D_{REV} can be considered for lower *ER*. The impossibility of installing

borehole extensometers at Subsection B1 (because of the locations of galleries) is another limitation of this study; however, Equation (**1**) is utilized by multiplying the mentioned safety factor.

D_{UREV} is calculated directly from extensometer deformations at REV, but we use the ratio of D_{UREV}/D_U for calculating D_{LREV}. However, this estimated D_{LREV} can be used at the design stage by multiplying a reasonable safety factor, considering the impossibility of evaluating rock mass behavior under loading at REV using alternative methods.

5 Conclusions

The main concerns in the studied slope are Zone B and three faults; we divide Zone B into two sections (B1 and B2). Zone B1 (about 10 m) and faulted rocks are geomechanically weak layers (D_{UREV} of 1.24-2.35 GPa), and reinforcement must be considered. Such D_{UREV} values are up to 80 % lower than the values measured through in situ tests.

Similar *ER*-D_{REV} relationships can be developed for various rock types, and soft computing methods (such as neural networks) can be employed to analyze the data and present universal equations for a category of rocks (like sedimentary formations). Therefore, removing extreme financial burdens, technical challenges, and environmental issues of in situ tests, in addition to coverage of the rock mass at the representative element volume, are advantages of utilizing *ER* tomography for evaluating the deformation moduli of faulted rock masses.

REFERENCES

Akbariforouz, M., Zhao, Q., Chen, K., Baghbanan, A., Narimani, R., & Zheng, C. (2022). Statistical study of squeezing for soft rocks based on factor and regression analyses of effective parameters. *International Journal of Rock Mechanics and Mining Sciences*, *163*. https://doi.org/https://doi.org/10.1016/j.ijrmms.2022.105306

Akbariforouz, M., Zhao, Q., Taherdangkoo, R., Baghbanan, A., Butscher, C., & Zheng, C. (2023). Prediction of tunnel squeezing in soft sedimentary rocks by geoelectrical data. *Environmental Earth Sciences*, *82*(7). https://doi.org/https://doi.org/10.1007/s12665-023-10835-0

Aksoy, C. O., Ogul, K., Topal, I., Ozer, S. C., Ozacar, V., & Posluk, E. (2012). Numerical modeling of non-deformable support in swelling and squeezing rocks. *International Journal of Rock Mechanics and Mining Sciences 52*, 61-70. https://doi.org/https://doi.org/10.1016/j.ijrmms.2012.02.008

Aladejare, A. E., & Idris, M. A. (2020). Performance analysis of empirical models for predicting rock mass deformation modulus using regression and Bayesian methods. *Journal of Rock Mechanics and Geotechnical Engineering*, *12*(6), 1263-1271. https://doi.org/https://doi.org/10.1016/j.jrmge.2020.03.007

Amirshahkarami, M., Vaziri-Moghaddam, H., & Taheri, A. (2007). Sedimentary facies and sequence stratigraphy of the Asmari Formation at Chaman-Bolbol, Zagros Basin, Iran. *Journal of Asian Earth Sciences*, *29*(5), 947-959. https://doi.org/https://doi.org/10.1016/j.jseaes.2006.06.008

Ammar, A. I., & Kamal, K. A. (2018). Resistivity method contribution in determining fault zone and hydro-geophysical characteristics of carbonate aquifer, eastern desert, Egypt. *Applied Water Science*, *8*(1), 1-27. https://doi.org/https://doi.org/10.1007/s13201-017-0639-9

Archie, G. E. (1947). The electrical resistivity is an aid in determining some reservoir characteristics. *AAPG Bulletin*, *31*(2), 350–366.

Barnard, H., & Heymann, G. (2015). The effect of bedding errors on the accuracy of plate load tests. *Journal of the South African Institution of Civil Engineering*, *57*(1), 67-76. https://doi.org/https://doi.org/10.17159/2309-8775/2015/v57n1a7

Bhatt, S., & Jain, P. K. (2014). Correlation between electrical resistivity and water content of sand-a statistical approach. *American International Journal of Research in Science, Technology, Engineering & Mathematics*, *6*(2), 115-121.

Brady, B. H. G., & Brown, E. T. (1993). *Rock mechanics for underground mining* (2nd ed.). Chapman & Hall.

Carpenter, B. M., Marone, C., & Saffer, D. M. (2011). Weakness of the San Andreas Fault revealed by samples from the active fault zone. *Nature Geoscience*, *4*(4), 251-254. https://doi.org/https://doi.org/10.1038/ngeo1089

Fattahi, H., Varmazyari, Z., & Babanouri, N. (2019). Feasibility of Monte Carlo simulation for predicting the deformation modulus of the rock mass. *Tunneling and Underground Space Technology*, *89*, 151-156.

ISBN: 978-81-989164-3-3 ISSN: 2582-3922

https://doi.org/https://doi.org/10.1016/j.tust.2019.03.024

Ghotbi Ravandi, E., Rahmannejad, R., Karimi-Nasab, S., & Sarrafi, A. (2017). Application of numerical modeling and genetic programming in hydrocarbon seepage prediction and control for crude oil storage unlined rock caverns. *Geofluids*, *2017*, 1-11. https://doi.org/https://doi.org/10.1155/2017/6803294

Hill, R. (1963). Elastic properties of reinforced solids: Some theoretical principles. *Journal of the Mechanics and Physics of Solids*, *11*(5), 357-372. https://doi.org/https://doi.org/10.1016/0022-5096(63)90036-X

Howland-Rose, A. W. (1981). *A report on a rapid reconnaissance magnetic induced polarization survey over a section of the Highland Valley*.

ISRM. (1998). Standard test method for determining the in situ modulus of deformation of rock mass using the rigid plate-loading method. *1.84 (Reapproved)*, 1–9.

ITASCA. (2002). *FLAC^{2D} user guide*. In Itasca Consulting Group, Inc.

Kahraman, S. (2022). Estimating the physicomechanical properties of pyroclastic rocks from electrical resistivity. *Pure and Applied Geophysics*, *179*(1), 301-309. https://doi.org/https://doi.org/10.1007/s00024-021-02898-6

Kahraman, S., & Yeken, T. (2010). Electrical resistivity measurement to predict uniaxial compressive and tensile strength for igneous rocks. *Bulletin of Materials Science*, *33*(6), 731-735. https://doi.org/https://doi.org/10.1007/s12034-011-0137-x

Khodabakhshi, A., & Mortazavi, A. (2018). Numerical modeling of determining in situ rock mass deformation modulus using the plate load test. *International Journal of Geological and Environmental Engineering*, *12*(8), 545–552. https://doi.org/https://doi.org/10.5281/zenodo.1474357

Ladanyi, B. (1987). Suggested method for deformability determination using flexible dilatometers. *International Journal of Rock Mechanics and Mining Sciences & Geomechanics Abstracts*, *24*(2), 123-134. https://doi.org/https://doi.org/10.1016/0148-9062(87)91042-4

Li, K., Pan, B., & Horne, R. (2015). Evaluating fractures in rocks from geothermal reservoirs using resistivity at different frequencies. *Energy*, *93*(P1), 1230-1238. https://doi.org/https://doi.org/10.1016/j.energy.2015.09.084

Liu, X., Beroza, G. C., & Li, H. (2023). Ambient noise differential adjoint tomography reveals fluid-bearing rocks near active faults in Los Angeles. *Nature Communications*, *14*(1), 6873. https://doi.org/https://doi.org/10.1038/s41467-023-42536-4

Militzer, H., Rosler, R., & Losch, W. (1979). Theoretical and experimental investigations for cavity research with geoelectrical resistivity methods. *Geophysical Prospecting*, *27*(3), 640–652. https://doi.org/https://doi.org/10.1111/j.1365-2478.1979.tb00991.x

Nia, H., & Mahdavi, S. A. (2020). Principles of geoelectrical methods. In *Physio-Geo*. https://www.researchgate.net/publication/346969879_principles_of_geoelectrical_methods_8_haifa_raniasari_haifania_2_principles_of_geoelectrical_methods

Palmström, A., & Singh, R. (2001). The deformation modulus of rock masses — comparisons between in situ tests and indirect estimates. *Tunneling and Underground Space Technology*, *16*(2), 115-131. https://doi.org/https://doi.org/10.1016/S0886-7798(01)00038-4

Pazha, H., Nasro, M., & Denya Agustina, R. (2019). Analysis of rock structures based on geoelectrical resistivity data of Wenner-Alpha configuration using Marquardt inversion method. *1st International Conference on Advance and Scientific Innovation*, *1175*(1), 12014. https://doi.org/https://doi.org/10.1088/1742-6596/1175/1/012014 (Journal of Physics Conference Series)

Peng, M., & Zhang, L. M. (2012). Analysis of human risks due to dam-break floods—part 1: a new model based on Bayesian networks. *Natural Hazards*, *64*(1), 903-933. https://doi.org/https://doi.org/10.1007/s11069-012-0275-5

Ranjbar, S., & Nasab, S. K. (2019). Determination of uniaxial compressive strength of granite rock samples using electrical resistivity measurement: NDT. *EAGE-GSM: 2nd Asia Pacific Meeting on Near Surface Geoscience & Engineering*, 22-26. https://doi.org/https://doi.org/10.3997/2214-4609.201900452

Ren, F., Zhang, J., Ouyang, Z., & Hu, H. (2021). Calculating elastic modulus for fractured rock mass using dimensional analysis coupled with numerical simulation. *Mathematical Problems in Engineering*, *2021*, 1-14. https://doi.org/https://doi.org/10.1155/2021/2803837

Rocscience. (2007). *RocLab manual*. In

Rolia, E., & Sutjiningsih, D. (2018). Application of the geoelectric method for groundwater exploration from the surface (A literature study). *AIP Conference Proceedings*, *1977*(1). https://doi.org/https://doi.org/10.1063/1.5042874

Sandler, J., Li, Y., Horne, R. N., & Li, K. (2009). Effects of fracture and frequency on resistivity in different rocks. *EUROPEC/EAGE Conference and Exhibition*. https://doi.org/https://doi.org/10.2118/119872-ms

Stavrakas, I., Anastasiadis, C., Triantis, D., & Vallianatos, F. (2003). Piezo stimulated currents in marble samples: Precursory and concurrent-with-failure signals. *Natural Hazards and Earth System Sciences*, *3*(3-4), 243-247. https://doi.org/https://doi.org/10.5194/nhess-3-243-2003

Su, O., & Momayez, M. (2017). Indirect estimation of electrical resistivity by abrasion and physicomechanical properties of rocks. *Journal of Applied Geophysics*, *143*, 23-30. https://doi.org/https://doi.org/10.1016/j.jappgeo.2017.05.006

Telford, W. M., Geldart, L. P., & Sheriff, R. E. (1990). Applied geophysics. https://doi.org/https://doi.org/10.1017/CBO9781139167932

Triantis, D., Stavrakas, I., Anastasiadis, C., Kyriazopoulos, A., & Vallianatos, F. (2006). An analysis of pressure stimulated currents (PSC) in marble samples under mechanical stress. *Physics and Chemistry of the Earth, Parts*, *47*(4-9), 234-239. https://doi.org/https://doi.org/10.1016/j.pce.2006.02.018

Wang, Z., & Gelius, L.-J. (2010). Electric and elastic properties of rock samples: a unified measurement approach. *Petroleum Geoscience*, *16*(2), 171-183. https://doi.org/https://doi.org/10.1144/1354-079309-013

ISBN: 978-81-989164-3-3 ISSN: 2582-3922